# Efficient prediction of wind and wave induced long-term extreme load effects of floating suspension bridges using artificial neural networks and support vector machines

Yuwang Xu[a], Aksel Fenerci[b], Ole Øiseth[c], Torgeir Moan[d]

[a]Asst. Professor, School of Naval Architecture, Ocean & Civil Engineering, Shanghai Jiao Tong University (corresponding author, Email: xuyuwang@sjtu.edu.cn)

[b] Postdoctoral researcher, Department of Structural Engineering, NTNU

[c] Professor, Department of Structural Engineering, NTNU

[d]Professor, Centre for Ships and Ocean Structures (CeSOS), NTNU; Centre for Autonomous Marine Operations and Systems (AMOS), NTNU

## Abstract

Long-term extreme load effects are one of the primary concerns in the design of civil and offshore structures. Such load effects can be evaluated using the accurate but computationally demanding full long-term method or the more efficient but approximate first-order and second-order reliability methods. Monte Carlo based methods enhanced with machine learning algorithms offer efficient alternatives to the traditional methods. Therefore, artificial neural networks and support vector machines along with Monte Carlo simulations are employed here in the prediction of long-term extreme load effects. A three-span suspension bridge with two floating pylons under combined wind and wave actions is used as a case study. The cumulative density functions of the long-term extreme values corresponding to a bending moment value due to vertical deflections at the critical position of the girder are calculated. It is then shown that the artificial neural network and support vector machine-based approaches require less computational effort and yield more accurate results than the first- and second-order reliability methods.

**Keywords**: artificial neural networks, support vector machines, first-order reliability method, second-order reliability method, long-term extreme load effects.

**Nomenclature**

| | | | |
|---|---|---|---|
| Environmental parameters | | Artificial nueral network | |
| $V$ | mean wind velocity | $\mathbf{w}$ | weight parameters |
| $I_u$, $I_w$ | horizontal and vertical turbulence intensity | $\mathbf{b}$ | bias parameters |
| | | $\alpha_0$, $\beta_0$ | objective function parameters |
| $H_s$, $T_p$ | significant wave height and peak wave period | $E_D$ | sum of the squared errors |
| | | $E_w$ | sum of the squares of the network weights |
| Reliability analysis methods | | $N$, $r$ | actual and effective number of weight and bias parameters |
| $g$ | limit state function | Support vector machine | |
| $X_d$ | extreme load effect in a short-term period with duration d | $\gamma$ | kernel parameter |
| | | $C$ | penalty parameter |

| | | | |
|---|---|---|---|
| $X_{crit}$ | a specified critical load effect | Operation symbol | |
| $\mathbf{s}$ | a vector of environmental parameters | | |
| $\mathbf{u}$ | standard normal random variables | $\Phi$ | CDF of a standard normal distribution |
| $\beta$ | reliability index | $\|\| \cdot \|\|$ | the norm of a vector |
| $T_{long}$,$T_{short}$ | long- and short-term periods | $\nabla(\cdot)$ | gradient of a function |
| $\Phi_{\mathbf{u}}$ | joint PDF of $\mathbf{u}$ | det(·) | determinant of a matrix |
| Abbreviations | | | |
| ANN | artificial neural networks | PDF | probability density function |
| CDF | cumulative distribution function | RMSE | root mean square error |
| FLM | full long-term method | SORM | second order reliability method |
| FORM | first order reliability method | SVM | support vector machines |
| MPP | most probable point | MCS | Monte Carlo simulations |

## 1 Introduction

The probability distribution of long-term extreme load effects is desired in the design of civil and offshore structures. In principle, the full long-term method (FLM), is an integration of short-term response statistics (e.g., distributions of all peaks, distributions of extreme values, or the mean upcrossing rate) over all possible environmental conditions and represents the most accurate approach. However, the FLM does not represent the most economical approach from a computational perspective because it must account for contributions from all possible short-term environmental conditions.

The long-term extreme load effects of structures can also be calculated using approximate reliability methods such as FORM and SORM (Rackwitz and Flessler, 1978; Zhao and Ono, 1999). In such methods, the point on the limit-state surface with the highest probability of occurrence (the so-called design point or the MPP) is sought after. Then, the limit state surface is approximated at the MPP by a linear surface in FORM, whereas it is replaced by its quadratic Taylor expansion in the case of SORM (Breitung, 1984; Der Kiureghian and De Stefano, 1991), making it more accurate if the failure surface is nonlinear. Ultimately, the performance of both methods hinges on the estimation of the MPP. To that end, several strategies has been developed over the years to search for it. Liu and Der Kiureghian (1991) compared several optimization algorithms to search for the MPP and found that the Hasofer-Lind and Rackwitz-Fiessler (HL-RF) method (Hasofer and Lind, 1974; Rackwitz and Flessler, 1978) and the modified HL-RF method outperformed others for the examples presented in their study. Later, Zhang and Kiureghian (1995) introduced an improved HL-RF method that showed better performance in terms of convergence in several examples (Santos et al., 2012; Zhang and Kiureghian, 1995).

More recently, machine learning approaches such as artificial neural network (ANN) and support vector machine (SVM) algorithms have been employed in structural reliability analysis. Machine learning algorithms are generally used to replace the implicit limit state function by a surrogate model. Therefore, they can be combined with both FORM, SORM and Monte Carlo methods. Several studies successfully used ANN-based MCS (Cardoso et al., 2008; Papadrakakis et al., 1996) in their reliability analyses, where others compared the results from ANN-based MCS and ANN-based FORM. On the other hand, several studies used SVM, either in connection with MCS (Hurtado, 2004; Rocco and Moreno, 2002) or FORM (Li et al., 2006; Zhao, 2008). The results showed remarkable accuracy and efficiency for the

basic examples presented. Although machine learning methods are shown to be applicable in FORM and SORM, their full potential is realized in Monte Carlo methods, where the computational effort is reduced significantly, and the accuracy is not compromised due to approximations of the limit state function.

ANNs can replace the implicit limit state function in the reliability problem, therefore avoiding time consuming simulations. An ANN consists of an input layer, hidden layer, and output layer that are connected by weights and bias parameters. The training of the network is then to find the optimum combination of these parameters to minimize the difference between the outputs and the corresponding target values. The feed-forward back-propagation (BP) network (Rumelhart et al., 1986; Vogl et al., 1988) is one of the most commonly used types. The direct way to solve this problem is through the widely used gradient descent, conjugate gradient (Charalambous, 1992) or quasi-Newton algorithms. The Levenberg-Marquardt (Hagan and Menhaj, 1994) algorithm that is based on the Newton-Raphson or Gauss-Newton methods shows a more robust and stable performance when employed in training neural networks. The Bayesian regulation method was introduced to neural network training by MacKay (1992a, 1992b) and adds the sum of the squared network parameters to the objective function in addition to the errors between the outputs and the targets. This approach has been shown to have good performance in controlling the so-called overfitting problem (Hirschen and Schäfer, 2006; Liang, 2005; Titterington, 2004).

SVM, which is essentially another powerful machine learning tool for data classification type of problems, can also be conveniently implemented into reliability analyses, if failure and safety are defined as two classes. The algorithm is based on the principle of structural risk minimization (Hurtado, 2004; Li et al., 2006; Pan and Dias, 2017) and usually requires a small amount of training data, which makes it computationally efficient (Pan and Dias, 2017).

Although ANN and SVM have been applied in some engineering-relevant reliability problems, most prior research has focused on the evaluation of performance and efficiency of the machine learning methods by applying them to simple benchmark examples. However, the applicability of such machine learning approaches to the prediction of the probability of long-term extreme load effects of complex structures is yet to be investigated.

In this paper, a new machine learning based Monte Carlo (MC) framework is developed to predict the cumulative distribution function (CDF) of the long-term extreme response of a floating suspension bridge under wind and wave actions. By replacing the implicit limit state function with surrogate models based on ANN and SVM, the efficiency of the MC method is increased significantly. In training of the algorithms, a strategy is devised to increase the accuracy of the models in the vicinity of the design point. The probability values and limit state surfaces obtained by ANN-based and SVM-based MC methods are then compared with the exact solutions obtained by the full long-term method and more efficient but approximate FORM and SORM. In the particular case study of the suspension bridge with floating pylons, which is characterized by a strongly nonlinear limit state function, FORM and SORM showed poor performance in estimation of the limit state surface and consequently the CDF of the long-term extreme response, whereas the ANN and SVM enhanced MC schemes showed great potential with respect to both computational efficiency and accuracy.

## 2 The floating suspension bridge concept

Figure 1 shows the model view of a three-span suspension bridge with two floating pylons proposed as a solution for crossing wide and deep fjords in Norway. The main cables are supported by two fixed pylons at each end of the bridge and two floating pylons in the middle of the bridge. The bottom part of the floating pylon is similar to tension leg platforms moored by four groups of tethers, providing a high stiffness in heave, pitch, and roll. Each of the main girder spans has a length of 1385 m, and the pylons are 198 m high and have a draft of 65 m. The water depth is 550 m and 450 m at the left and

right floating pylons, respectively. A comprehensive finite element model of the bridge, as displayed in Figure 1, is used in the dynamic analysis. The girder, main cable, tethers, hangers, and pylons are modeled using beam elements. More details about the finite element model of the bridge are presented in Gong and Halden (2016).

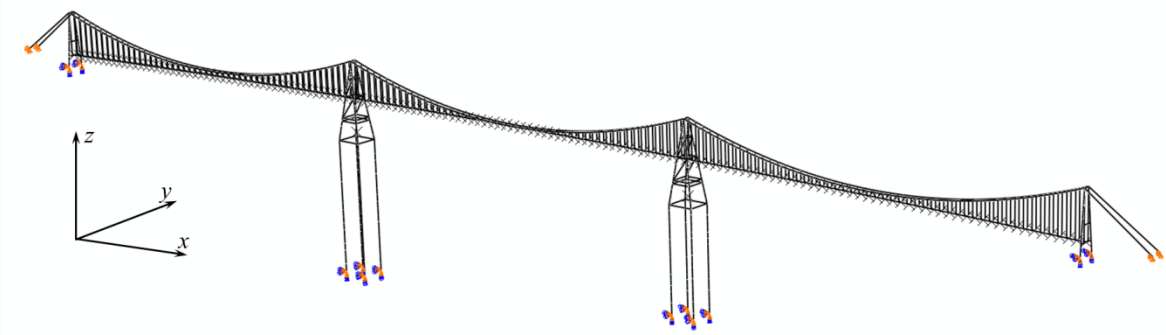


Figure 1 Finite element model of the three-span suspension bridge with two floating pylons

## 3 Prediction of the long-term extreme load effects

### 3.1 Long-term description of the wind and wave fields

In prediction of the long-term extreme load effects of complex structures, a long-term description of the environmental conditions is needed. The long-term condition can be considered as a sequence of stationary short-term (1 hour) conditions characterized by the $H_s$, $T_p$ and $V$. Here, due to lack of usable site measurements, a scaled dataset from the North Sea is used, where the wave height and the period are divided by 2.5 and $\sqrt{2.5}$, respectively to match the preliminary surveys at the site, where the mean wind velocity is kept as it is (Li et al., 2015). The marginal distribution of the mean wind velocity $V$ and the conditional distribution of significant wave height $H_s$ given the mean wind velocity are presented using a two-parameter Weibull distribution model. Moreover, the conditional distribution of peak wave period $T_p$ given both the mean wind velocity and the significant wave height is fitted to a lognormal distribution. The wind and waves are assumed to be colinear and perpendicular to the bridge axis. Table 1 lists the assumed parameters (Johannessen et al., 2002; Li et al., 2015) and the expressions of for the probability distributions of environmental parameters are given below:

$$f_V(v)=\frac{\alpha_V}{\beta_V}\left(\frac{v}{\beta_V}\right)^{\alpha_V-1}\cdot\exp\left(-\left(\frac{v}{\beta_V}\right)^{\alpha_V}\right) \tag{1}$$

$$f_{H_s|V}(h_s|v)=\frac{\alpha_{Hs}}{\beta_{Hs}}\left(\frac{h_s}{\beta_{Hs}}\right)^{\alpha_V-1}\cdot\exp\left(-\left(\frac{h_s}{\beta_{Hs}}\right)^{\alpha_{Hs}}\right),\quad \alpha_{Hs}=a_1+a_2\cdot v^{a_3};\quad \beta_{Hs}=b_1+b_2\cdot v^{b_3} \tag{2}$$

$$f_{T_p|V,H_s}(t_p|v,h_s)=\frac{1}{\sqrt{2\pi}\sigma_{\ln(T_p)}t_p}\cdot\exp\left[-\frac{1}{2}\left(\frac{\ln(t_p)-\mu_{\ln(T_p)}}{\sigma_{\ln(T_p)}}\right)^2\right],$$

$$\mu_{\ln(T_p)}=\ln\left(\frac{\mu_{T_p}}{\sqrt{1+\upsilon_{T_p}^2}}\right),\quad \sigma^2_{\ln(T_p)}=\ln(1+\upsilon^2_{T_p}),\quad \upsilon_{T_p}=\frac{\sigma_{T_p}}{\mu_{T_p}} \tag{3}$$

$$\mu_{T_p}=(e_1+e_2\cdot h_s^{e_3})\cdot\left[1+\theta\left(\frac{v-(f_1+f_2\cdot h_s^{f_3})}{f_1+f_2\cdot h_s^{f_3}}\right)^{\gamma}\right];\qquad \upsilon_{T_p}=k_1+k_2\cdot\exp(k_3h_s)$$

Table 1 Parameters for the marginal distribution of V and the conditional distributions of $H_s$ and $T_p$

| $\alpha_V$ | $\beta_V$ | $\theta$ | $\gamma$ | $a_1$ | $a_2$ | $a_3$ | $b_1$ | $b_2$ | $b_3$ |
|---|---|---|---|---|---|---|---|---|---|
| 2.209 | 9.409 | -0.255 | 1.0 | 2.136 | 0.013 | 1.709 | 1.816 | 0.024 | 1.787 |
| $e_1$ | $e_2$ | | $e_3$ | $f_1$ | $f_2$ | $f_3$ | $k_1$ | $k_2$ | $k_3$ |
| 8.0 | 1.938 | | 0.486 | 2.5 | 3.001 | 0.745 | -0.001 | 0.316 | -0.145 |

### 3.2 Wind- and wave-induced responses

In calculation of the response of the suspension bridge with floating pylons, namely the section bending moments along the girder, combined wind and wave actions are considered. The wind actions consist of a time-invariant component due to the mean wind velocity, a stationary dynamic component due to turbulence and self-excited forces induced by the motion of the girder. The wave actions include the radiation force generated by the motion of the submerged part of the pylons and the first-order wave excitation force. The second-order excitation force, viscous drag damping forces on the pylons and the tethers and possible excitations due to vortex shedding are out of the scope of this study. Furthermore, the nonlinear buffeting forces are disregarded due to its negligible contribution to the overall response (Xu et al., 2018a) and nonlinear aerodynamics are not modeled owing to the linear nature of the bridge section that is used. The equation of motion is solved by multi-mode frequency domain method (Xu et al., 2018a). The standard deviation of the bending moment due to vertical deflection at the critical position of the girder (with the maximum bending moment) under various combinations of wind velocity, wave height, and peak period are shown in Figure 2. As expected, the sea states with greater significant wave height induce larger wave excitation forces and correspondingly larger section moments. However, the structural response is not necessarily larger with the increasing wind speed under large wave heights. This is due to larger aerodynamic damping under stronger winds. In addition, the variation in the section moments depends strongly on the wave period. The peaks in the bending moment due to vertical deformation are located within the wave period range from 3 s to 8 s, which contains several vertical natural modes. Given a specified environmental condition, the conditional CDF of the extreme value of the section moment due to vertical deflection in the girder in a short-term period can be written as follows (Naess and Moan, 2012):

$$F_{X_d|\mathbf{s}}(x\,|\,\mathbf{s}) = \exp\left\{-\nu_x^+(0\,|\,\mathbf{s})T_{short}\exp\left(-\frac{x^2}{2\sigma_x(\mathbf{s})^2}\right)\right\},\quad \nu_x^+(0\,|\,\mathbf{s}) = \frac{1}{2\pi}\frac{\sigma_{\dot{x}}(\mathbf{s})}{\sigma_x(\mathbf{s})} \tag{4}$$

where $\sigma_x$ and $\sigma_{\dot{x}}$ are the standard deviations of the response process and its derivative and $\nu_x^+(0\,|\,\mathbf{s})$ denotes the mean zero-upcrossing rate.

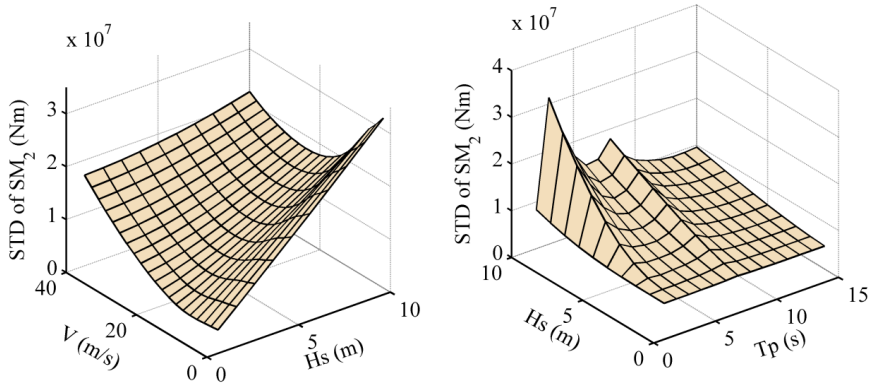


(a) Tp=8 s (b) V=20 m/s

Figure 2 Standard deviation (STD) of the bending moment due to vertical deformation

### 3.3 The full long-term method

As stated earlier, the long-term condition (i.e. 100 years) is a sequence of many short-term intervals (1 hour), which are characterized by a set of environmental parameters $\mathbf{s}=\left[V,H_s,T_p\right]$. Denoting the extreme load effect in a short-term period as $X_d$, the CDF of the extreme load effect in the long-term period can be written as

$$F_{X_d}(x)\approx\int_{\mathbf{s}}F_{X_d|\mathbf{S}}(x\,|\,\mathbf{s})f_{\mathbf{S}}(\mathbf{s})d\mathbf{s} \tag{5}$$

where $f_S(\mathbf{s})$ and $f_{X_d|\mathbf{s}}(x|\mathbf{s})$ refer to the occurrence probability of a specified environmental condition ***s*** and the CDF of the extreme response in a short-term period given this environmental condition (Eqn. (4)), respectively. It should be noted that the formulation based on the short-term extremes is used here; however, formulations based on other response statistics, such as peak values or upcrossing rate can also be used (Naess and Moan, 2012). Direct integration of the above expression is called the full long-term method (FLM). In other words, the FLM is an integration of all possible short-term response statistics weighted by their probability of occurrence. The CDF of the long-term extreme response can then be obtained using

$$F_{\hat{X}}(x)=\left[F_{X_d}(x)\right]^{T_{long}/T_{short}} \tag{6}$$

The relation in Eqn. (5) can also be formulated as a structural reliability problem. To that end, introducing $X_{\text{crit}}$ as an arbitrary critical load effect, a limit state function is written in the form (Madsen et al., 2006)

$$g(\mathbf{s};X_d(\mathbf{s}),X_{\text{crit}})=X_{\text{crit}}-X_d(\mathbf{s}) \tag{7}$$

The integration then can be rewritten as

$$p_f(X_{\text{crit}})\approx\int_{\mathbf{s}}\int_{g(\mathbf{s};X_d,X_{\text{crit}})\le 0}f_{X_d|\mathbf{s}}(x|\mathbf{s})dx\,f_S(\mathbf{s})d\mathbf{s} \tag{8}$$

using the limit state function. Here, $p_f(X_{\text{crit}})$ is the probability that the limit state criteria is violated ( $X_{\text{crit}}-X_d(\mathbf{s})\le 0$ ), commonly referred to as the probability of failure in structural reliability analysis. Notice that this is equivalent to 1- $F_{X_d}(X_{\text{crit}})$. The expression can be further simplified defining a new vector $\boldsymbol{\omega}=\left[\mathbf{s};X_d\right]$ as

$$p_f(X_{\text{crit}})\approx\int_{g(\boldsymbol{\omega},X_{crit})\le 0}f_{\boldsymbol{\omega}}(\boldsymbol{\omega})d\boldsymbol{\omega} \tag{9}$$

which is the familiar form of the generalized reliability problem.

### 3.4 First-order reliability method (FORM)

Directly solving Eqn. (9) is not efficient; therefore, it is often approximated using FORM. First, the variables are transformed into the standard normal space (the so-called u-space), applying the Rosenblatt transform (Rosenblatt, 1952). The transformation uses conditional CDFs of the variables in a stepwise manner as follows:

$$
\begin{aligned}
F_V(v) = \Phi(u_1) \quad &\Leftrightarrow \quad u_1 = \Phi^{-1}\left[F_V(v)\right] \\
F_{H_s|V}(h_s|v) = \Phi(u_2) \quad &\Leftrightarrow \quad u_2 = \Phi^{-1}\left[F_{H_s|V}(h_s|v)\right] \\
F_{T_p|H_s,V}(t_p|h_s,v) = \Phi(u_3) \quad &\Leftrightarrow \quad u_3 = \Phi^{-1}\left[F_{T_p|H_s,V}(t_p|h_s,v)\right] \\
F_{X_d|T_p,H_s,V}(x_d|t_p,h_s,v) = \Phi(u_4) \quad &\Leftrightarrow \quad u_4 = \Phi^{-1}\left[F_{X_d|T_p,H_s,V}(x_d|t_p,h_s,v)\right]
\end{aligned} \tag{10}
$$

and it preserves probability so that

$$
\int_{g(\boldsymbol{\omega})\le 0} f_{\boldsymbol{\omega}}(\boldsymbol{\omega})d\boldsymbol{\omega} = \int_{g(\mathbf{u};X_{\text{crit}})<0} \phi_{\mathbf{U}}(\mathbf{u})d\mathbf{u} \tag{11}
$$

where $\phi_{\mathbf{U}}$ is the joint probability density function of the standard normal random variables. After the transformation, the failure probability reads:

$$
p_f(X_{\text{crit}}) = \int_{g(\mathbf{u};X_{\text{crit}})<0} \phi_{\mathbf{U}}(\mathbf{u})d\mathbf{u} \tag{12}
$$

FORM assumes that the limit state function $g(\mathbf{u};X_{\text{crit}})=0$ in the u-space can be approximated linearly by a first-order Taylor expansion. Prior to this assumption, there is no loss of accuracy. Furthermore, to guarantee that the first-order expansion will be as accurate as possible, the Taylor expansion of the limit state function is obtained at the MPP which provides the greatest contribution to the failure probability. In the u-space, searching for the MPP is equivalent to minimizing the distance from the origin to the known failure surface defined by $g(\mathbf{u};X_{\text{crit}})=0$ (Du, 2005). Therefore, the basic idea of FORM is as follows:

$$
\text{Given } X_{\text{crit}}\text{, find } \beta = \min(\|\mathbf{u}\|) \text{ subject to } g(\mathbf{u};X_{\text{crit}})=0
$$

where $\|\cdot\|$ stands for the norm of a vector, and $\beta$ is the distance from the origin to the MPP. When the limit state function is linearly expanded at the MPP in the u-space, the probability of exceeding $X_{\text{crit}}$ over a short-term period is defined as follows (Haver and Winterstein, 2009):

$$
p_f = \int_{g(\mathbf{u};X_{\text{crit}})<0} \phi_{\mathbf{U}}(\mathbf{u})d\mathbf{u} = 1-\Phi(\beta) \tag{13}
$$

The design point can be obtained using the HL-RF method (Liu and Der Kiureghian, 1991):

$$
\mathbf{u}^{k+1} = \frac{1}{\left\|\nabla \mathrm{g}(\mathbf{u}^k)\right\|^2}\left[\nabla \mathrm{g}(\mathbf{u}^k)\mathbf{u}^k - \mathrm{g}(\mathbf{u}^k)\right]\nabla \mathrm{g}(\mathbf{u}^k)^T \tag{14}
$$

Here, $\nabla(\mathrm{g}(\mathbf{u}^k))$ denotes the gradient of the limit state function evaluated at point $\mathbf{u}^k$. The design point is obtained when Eqn. (14) converges, i.e., $\left\|\mathbf{u}^{k+1}-\mathbf{u}^k\right\| / \left\|\mathbf{u}^{k+1}\right\| \le \varepsilon$, where $\varepsilon$ is the convergence tolerance.

The probability of the extreme section bending moment due to vertical deflection of the girder not exceeding a bending moment value of 50.4 MNm is calculated using FORM. The moment value is taken from Xu et al. (2018), which represents the 100-year load effect. An improved HL-RF method is used to obtain the design point, since the iterations oscillate among several conditions without convergence when the HL-RF is used. The details of the improved HL-RF method are given in (Liu and Der Kiureghian, 1991; Zhang and Kiureghian, 1995). 12 iterations have been performed before converging to the point $u_1$=4.23, $u_2$=0.497, $u_3$=-0.281, and $u_4$=1.84, which is very close to the true

design point (MPP), obtained using the full long-term method (Xu et al., 2018b). Here, $u_1$, $u_2$, $u_3$, and $u_4$ are variables in the Gaussian space transformed from the distribution or conditional distribution of the mean wind velocity, significant wave height, peak wave period, and short-term extreme responses. The results correspond to a mean wind velocity of 28.3 m/s, a significant wave height of 4.61 m, and a peak wave period of 8.13 s in the physical space. The failure surface approximated by FORM is plotted along with the exact failure surface in Figure 3(a) for the sake of comparison. In the figure, a fixed value for $u_1$ coincident with the true design point was assumed for the sake of visualizing the 4-d failure surface in a 3-d plot. Clearly, the first-order approximation fails to represent the true failure surface. The non-exceedance probability (CDF value) of the long-term extreme bending moment corresponding to the bending moment value of 50.42 MNm based on FORM is 0.228 with an error of 39.5% compared with the value 0.396 that is obtained from the full long-term method.

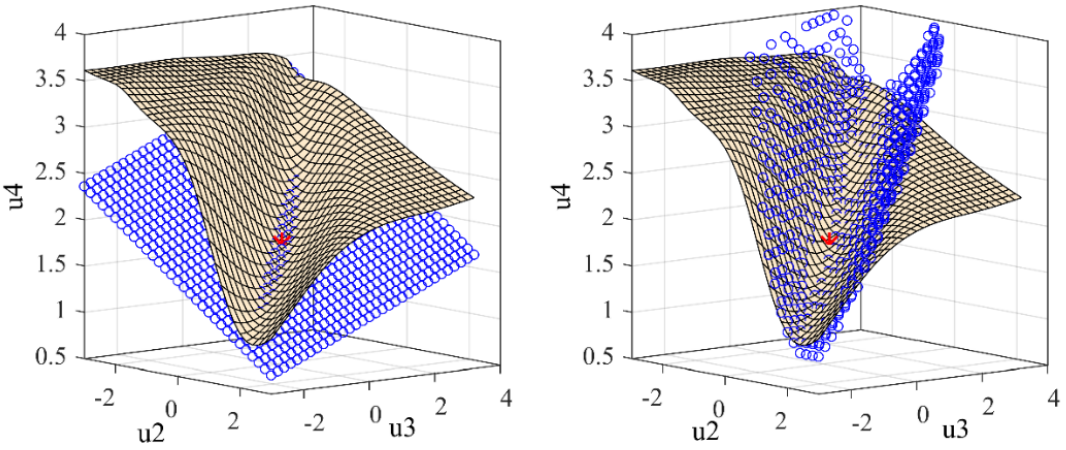


(a) FORM (b) SORM

Figure 3 Comparison of the failure surface based on FORM and SORM with the exact solution. (o: Failure surface based on FORM; ▭: Exact failure surface; * Design case)

### 3.5 Second-order reliability method (SORM)

SORM approximates the limit state function $g(\mathbf{u}) = 0$ in the u-space via a second-order Taylor expansion at the MPP. The approximation of the limit state function can be written as follows (Naess and Moan, 2012):

$$g_u(\mathbf{u}) = g(\mathbf{u}^*) + (\mathbf{u} - \mathbf{u}^*)^T \nabla g(\mathbf{u}^*) + \frac{1}{2}(\mathbf{u} - \mathbf{u}^*)^T \mathbf{H}(\mathbf{u}^*)(\mathbf{u} - \mathbf{u}^*) \tag{15}$$

Here, $\mathbf{H}(\mathbf{u}^*)$ is the Hessian matrix of the limit state function at the MPP with respect to the Gaussian variables. The failure probability based on Breitung's asymptotic approximation can be written as follows (Breitung, 1984):

$$p_f \approx \Phi(-\beta) \prod_{i=1}^{n-1} (1 - \beta\kappa_i)^{-1/2} \tag{16}$$

where $\kappa_i$ is the $i$th main curvature of the limit state function at the MPP. $\Phi(-\beta)$ is the failure probability obtained by FORM. Therefore, $\prod_{i=1}^{n-1} (1 - \beta\kappa_i)^{-1/2}$ is also called the SORM factor.

The non-exceedence probability of the extreme section bending moment due to vertical deflection of the floating suspension bridge girder is also evaluated using SORM. The value of the CDF corresponding to the bending moment of 50.4 MNm is found to be 0.441. Compared to the exact value of 0.396 from the full long-term method, this yields an error of 10.3%, which is a significant improvement compared to FORM. The failure surface approximated using SORM is shown in Figure 3(b). Although the approximated failure surface is superior to FORM, it still lacks accuracy further from the design point.

### 3.6 Monte Carlo Method Enhanced with Machine Learning Algorithms

The probability distribution of the long-term extreme load effects can also be obtained using Monte Carlo simulations. In that case, the expression of the CDF can be written as follows (Naess and Moan, 2012):

$$F(X_{crit}) = \left( \frac{m(X_d^{MC} \leq X_{crit})}{M} \right)^{T_{long}/T_{short}} \tag{17}$$

Where $X_d^{MC}$ are the Monte Carlo simulated short-term extremes, $m(X_d^{MC} \leq X_{crit})$ is the number of cases where the output is smaller than $X_{crit}$, and $T_{long}$ and $T_{short}$ are the durations of the long-term and short-term periods, which in this case are 100 years and 1 hour, respectively. This framework requires many simulations giving the output $X_d^{MC}$ for the set of $M$ randomly generated samples of the environmental variables $H_s$, $T_p$ and $V$. For each combination of the environmental variables, random samples of $X_d^{MC}$ can be drawn using the conditional distribution given in Eqn. (4), after the standard deviation of the load effect and its derivative is calculated in frequency domain. This means an exhausting number of calls to the multimode frequency domain routine is necessary, which is time consuming. However, if machine learning algorithms such as ANNs or SVMs are trained using a limited number of simulations and used instead of the response calculation routine, a significantly more efficient framework can be achieved.

Taking advantage of the equality given in Eqn. (11) and the Rosenblatt transform, the random samples can also be generated in the u-space directly, which is desirable due to the its convenience. For a random set consisting of independent Gaussian variables $u_1$, $u_2$, $u_3$ *and* $u_4$ described in (10), the Monte Carlo simulated short-term extreme response is written as

$$X_d^{MC} = F_{X_d|\mathbf{s}}^{-1}(\Phi(u_4)) \tag{18}$$

Here, it is noticed that a unique $X_d^{MC}$ is obtained for each random set of u values. However, the evaluation of the function $F_{X_d|\mathbf{s}}^{-1}(x|\mathbf{s})$ needs calculation of the standard deviations of the load effect and its derivative for each combination of $u_1$, $u_2$ and $u_3$. This can be avoided by training machine learning algorithms that take the random variables $u_1$, $u_2$, $u_3$ *and* $u_4$ as input and give the corresponding $X_d^{MC}$ as output.

#### 3.6.1 Training cases

The efficiency and accuracy of the machine learning algorithms are highly dependent on the training cases; therefore, they should be selected carefully. Since the location of the design point is unknown prior to training of the algorithms, the generated training cases are suggested to cover most of the u-space. Therefore, $u_1$, $u_2$, and $u_3$ are selected in the ranges [-1, 5], [-2, 5], and [-5, 5], respectively, whereas the Gaussian variable u4 is selected in the range [-5, 5]. It should be noted that once $u_1$, $u_2$, and $u_3$ are known, Eqn. (18) explicitly defines the relationship between $u_4$ and $X_d^{MC}$. This means that the response prediction routine will be called only for unique combinations of $u_1$, $u_2$, and $u_3$, where many values of

$u_4$ can be used in training without much computational effort. For the initial training of the network, it is desired that the training data is uniformly distributed in the u-space to avoid large errors in the regions with less data. Therefore, the $u_1$-$u_2$-$u_3$ parameter space is divided into 5×5×5 equal regions, and one training case is generated for each region by assuming that they follow a uniform distribution in the region, as presented by the blue circles in Figure 4. The total number of calls to the response prediction routine therefore adds up to 5x5x5 = 125. Using 101 values of $u_4$, the size of the training data becomes 5x5x5x101 = 12625 points, of which 10% is reserved as validation set and the rest is used as the training set.

### 3.6.2 Artificial neural networks

Figure 5 shows a feed-forward back-propagation ANN with three layers, i.e., input layer, hidden layer, and output layer. The network can have one or more hidden layers depending on the complexity of the research problem. One hidden layer is sufficient for the case study in this paper. Each layer contains several neurons that are connected by the weight parameters $w$. A bias parameter $b$ is used to modulate the element output. Typically, the number of neurons in the hidden layer is chosen via trial and error. The training of the neural network is basically to update the weight and bias parameters to minimize the network errors which are defined as the difference between the output and target values. The Bayesian regularization algorithm is employed in in training due to its superiority in avoiding overfitting. The algorithm minimizes the combination of squared errors and weights as follows:

$$\min \quad \beta_0 E_D + \alpha_0 E_W \tag{19}$$

Here, $E_D$ is the sum of squared errors and $E_W$ is the sum of squares of the network weights. $\alpha_0$ and $\beta_0$ denote the objective function parameters representing the emphasis of reducing the weight size or minimizing the network errors during the training.

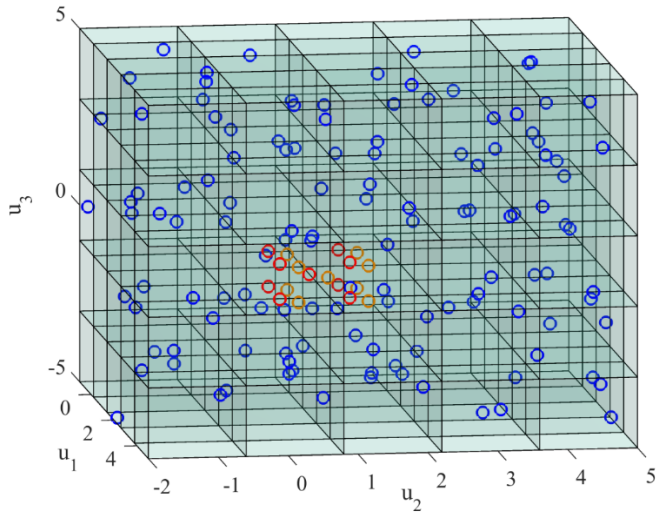


Figure 4 Values of $u_1$, $u_2$, and $u_3$ of the training and test cases (o refers to the training cases, o refers to the test cases in ANN, and o represents the test cases in SVM)

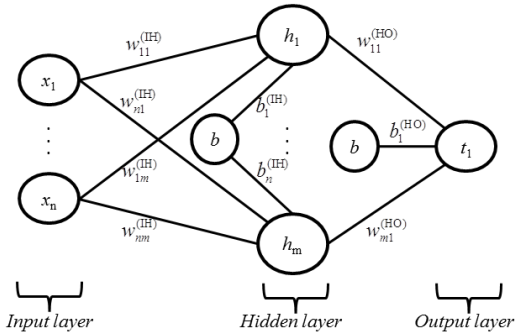


Figure 5 Structure of an n-m-1 neural network

The workflow of the prediction of the long-term extreme load effects using ANNs is illustrated in Figure 6. Training of the network was performed using the MATLAB toolbox Neural Net Fitting. In the case study, the inputs are the Gaussian variables transformed from the distribution or conditional distribution of the environmental parameters (such as mean wind velocity, significant wave height and peak wave period in this paper) and short-term extreme responses based on the Rosenblatt transform algorithm (Rosenblatt, 1952), as represent as **u** in Eqn. (12). The targets are the values of short-term extreme responses which are referred as $X_d$ in Eqn. (7). Each combination of **u** corresponds to a unique value of $X_d$. By mapping the inputs to the targets in the MATLAB toolbox, the weight and bias parameters connecting different layers of the network are obtained. In order to optimize the network, step 3 is introduced, which finds the design point (FORM-MPP) using the roughly trained neural network and generates several test cases around the design point for re-training the network. Finally, in step 4, the re-trained neural network is combined with the Monte Carlo method to predict the probability distribution of long-term extreme load effects.

Although it is not very likely for the problem considered here, it is possible that the reliability problem accommodates more than one design point due to a highly nonlinear limit state function in the u-space. In such a case, MC simulations will still yield accurate results. However, it is advised that the amount of training data is increased, where the step 3 should either be removed or modified to search for multiple design points, using the established methods of structural reliability (Der Kiureghian and Dakessian, 1998).

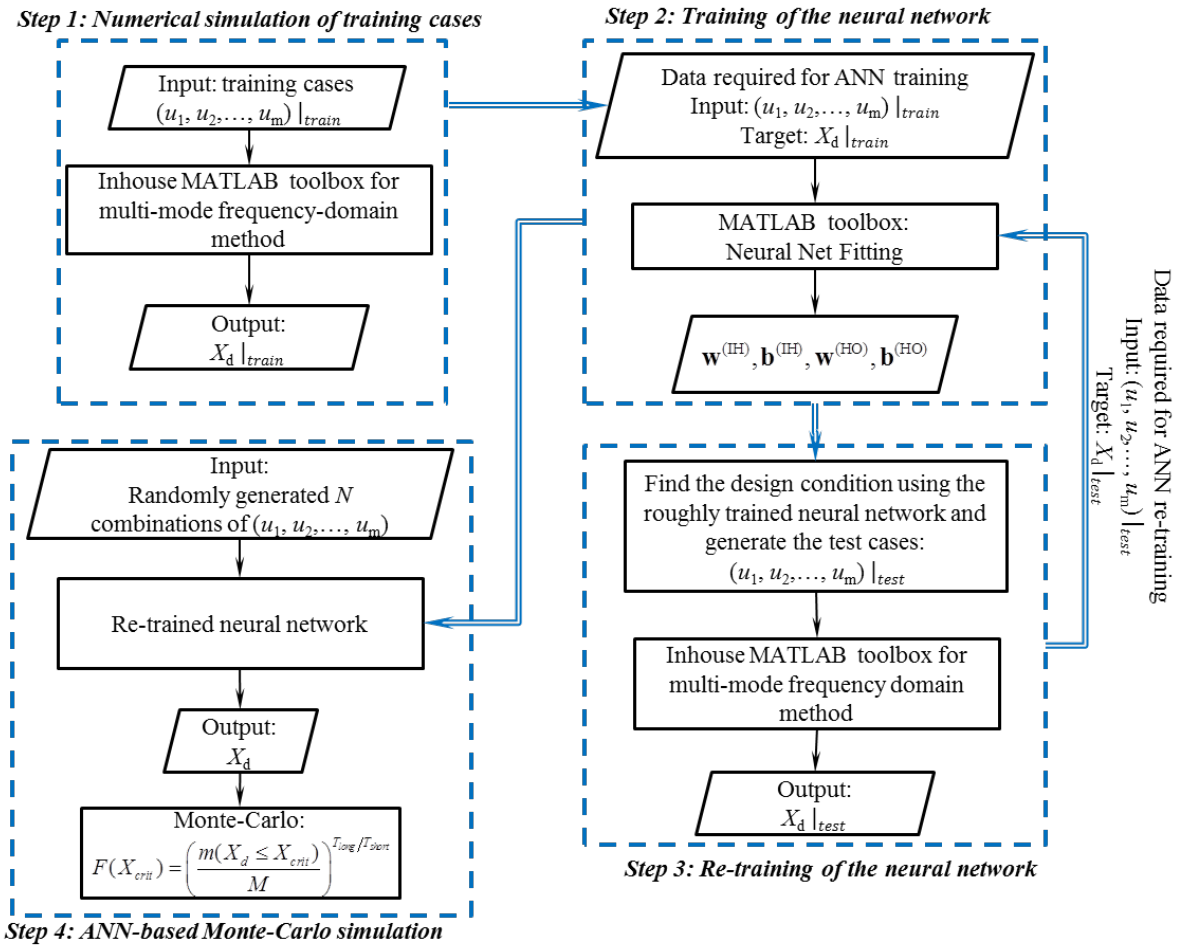


Figure 6 The procedure for the application of an ANN in predicting long-term extreme load effects

### 3.6.2.1 Determination of the number of neurons

To an extent, the performance of an ANN is dependent on the number of neurons in the hidden layer and the initial values of the weight and bias selected. For the case study considered, the training process does not require extensive computational effort. Therefore, a simple trial and error scheme is applied to determine the optimal number of neurons in the hidden layer. The number of neurons is then determined based on the effective number of parameters $r$ as well as based on the sum of square errors between the outputs and the targets (Dan Foresee and Hagan, 1997). The actual number of weight and bias parameters in the neural network is represented by $N$, whereas the effective number, $r$, indicates how many of the weight and bias parameters are effectively used. If $r$ is very close to $N$, then there may be an insufficient number of neurons or hidden layers. More neurons should be added until $r$ no longer increases. Several networks with different numbers of neurons in the hidden layer are trained, and Table 2 lists the corresponding squared errors and the actual and effective number of the parameters. It is observed that the sum of the squared errors always converges as the number of neurons exceeds 40. Moreover, the effective number of parameters also remains at approximately 240 and does not increase significantly with increasing number of neurons. Therefore, the network with 40 neurons in the hidden layer is considered as the optimum choice for this nonlinear problem, given that the simplest possible network with no loss of accuracy is sought after.

Table 2 The sum of the squared errors and the actual and effective number of parameters in the neural networks with different numbers of neurons in the hidden layer

| Number of neurons | 10 | 20 | 30 | 40 | 50 | 60 | 70 |
|---|---|---|---|---|---|---|---|
| $E_D$ | 2.07 | 0.440 | $7.94 \cdot 10^{-2}$ | $6.35 \cdot 10^{-2}$ | $6.51 \cdot 10^{-2}$ | $6.37 \cdot 10^{-2}$ | $6.36 \cdot 10^{-2}$ |
| N | 61 | 121 | 181 | 241 | 301 | 361 | 421 |
| r | 56.4 | 117 | 173 | 233 | 242 | 244 | 234.6 |

#### 3.6.2.2 Selection and updating of the neural networks

Twenty ANNs with 40 neurons in the hidden layer, each with different initial weight and bias parameters are trained using the Bayesian regularization algorithm. The condition at the mean position of the MPP predicted by the twenty networks, and another eight conditions at the corners of a cube with a center at the MPP and a length of one, is displayed by the red circles in Figure 4. These 9 conditions are selected as the first three Gaussian coordinates of the test cases. The average value of $u_4$ is 1.89; thus, the fourth coordinate of the inputs is selected in the range [1.39, 2.39] with an interval of 0.1, giving 11 values of $u_4$. The root-mean-square error (RMSE) of the predicted short-term extreme values of the section moment for the test cases compared to the exact solutions is used as the criterion to judge which network has the best performance. The RMSE is defined as follows:

$$RMSE = \sqrt{\frac{1}{n}\sum_{i=1}^{n}(X_d^{(\text{true})} - X_d^{(\text{pred})})^2} \tag{20}$$

Here, $X_d^{(\text{pred})}$ is the predicted value of the section moment using the trained neural network, and $X_d^{(true)}$ is the target value; $n$ is the number of the test cases. The predicted short-term extreme values of the section moment of the 9×11 test cases based on three of the networks are compared with the true results, as shown in Figure 7. The trial-and-error scheme is used to identify the network with optimal initial parameters, i.e. giving the least error (RMSE). The third network shown in Figure 7 introduces the minimal RMSE and is selected to predict the distribution of the long-term extreme values of the section moment due to vertical deflections. At the end of the training, the total number of structural analyses that were performed is only 5x5x5 + 9 = 136.

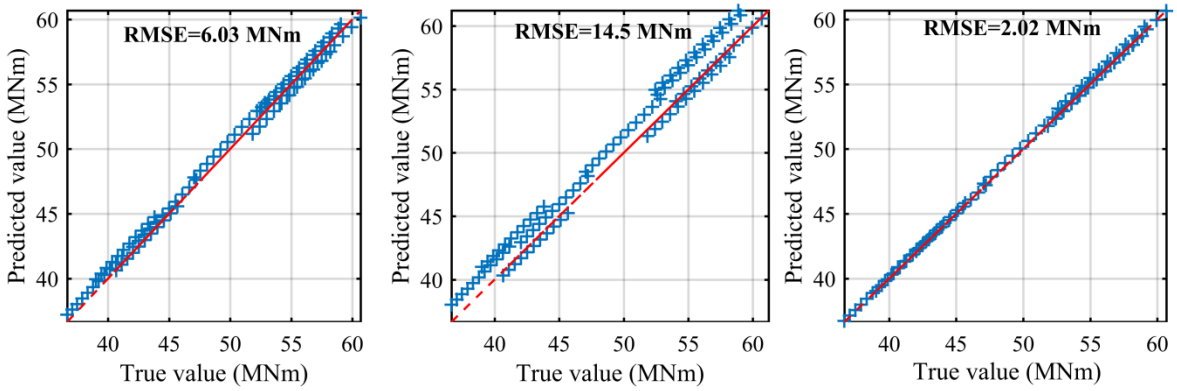


Figure 7 Comparison of the predicted values of the test cases to the true values applying different neural networks with different initial weight and bias parameters

#### 3.6.2.3 ANN-based Monte Carlo simulation

The predicted failure surface, defined as the section moment being equal to 50.42 *MNm*, match quite well with the exact surface, as shown in Figure 8. According to the ANN-based Monte Carlo simulation, the CDF value corresponds very well with the full long-term method over the entire range of the long-term extreme values, as shown in Figure 9, and the probability of the bending moment not exceeding the value of 50.42 *MNm* in 100 years is calculated as 0.3985 with an error of 0.63%.

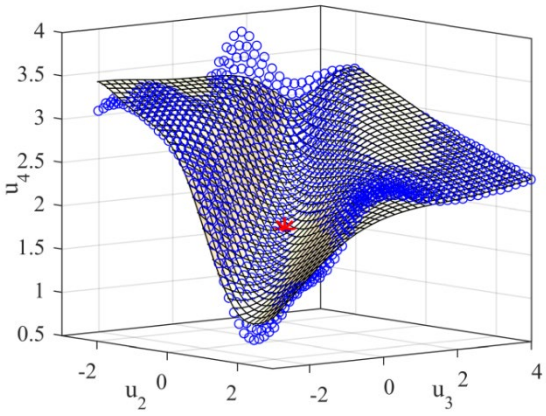


Figure 8 Comparison of the failure surface between the ANN and exact solutions. The legend of the figure is the same as in Figure 9.

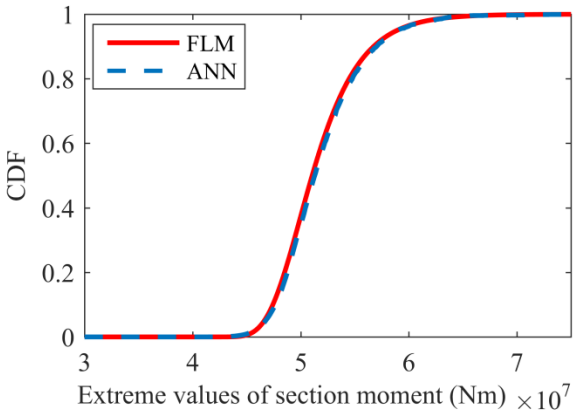


Figure 9 Comparison of the CDF of the long-term extreme response between the ANN with FLM solutions

### 3.6.3 Support vector machine

Given a set of training data, $(\mathbf{x}_1, y_1)$, $(\mathbf{x}_2, y_2), \cdots$, and $(\mathbf{x}_n, y_n)$ ($\mathbf{x}_i \in R^p$, $y_i \in \{-1, +1\}$ and '-1' and '1' represent two different categories), the main purpose of SVM is to find a hyperplane in a high- or infinite-dimensional space to separate the training data as different classes. In reliability analysis, the two classes refer to 'safety' and 'failure' domains. In the case study of the probability distribution of extreme load effects, the two classes are the short-term extreme response value exceeding or not exceeding a specified critical value. The hyperplane, named as 'failure surface' in the long-term analysis, is usually expressed as follows:

$$\mathbf{w}^T \mathbf{x} + b = 0 \tag{21}$$

Here, $\mathbf{w}$ is the orthogonal vector to the hyperplane, and $b$ is the bias term. The optimization problem searching for appropriate $\mathbf{w}$ and $b$ values can be formulated as maximizing the margin, which is also equal to minimizing $\|\mathbf{w}\|$ with a constraint to guarantee that all training data are on the correct side of the hyperplane. To control overfitting, classification errors should be allowed, which can be expressed as:

$$\min \ \frac{1}{2}\|\mathbf{w}\|^2 + C\sum_{i=1}^{n}\xi_i, \ \text{subject to } y_i\left[\mathbf{w}^T\mathbf{x}_i + b\right] \geq 1 - \xi_i, \ \mathrm{i} = 1, 2, \cdots, \mathrm{n} \tag{21}$$

Here, $\xi$ represent the distance of the training data from the functional margin. It is positive when the $i$th training point is in a wrong position; otherwise, it is zero. $C$ is the parameter defined by the user to assign the penalty to the classification errors.

When the training data are required to be separated by a nonlinear hyperplane, the optimization problem can be solved by mapping the variables to a higher dimensional space, $\mathbf{x} \rightarrow \phi(\mathbf{x})$, as shown in Figure 10(b). This mapping function is called the kernel function $k\left(\mathbf{x}_i, \mathbf{x}_j\right) = \left\langle \phi(\mathbf{x}_i) \cdot \phi(\mathbf{x}_j) \right\rangle$. Radial basis function is one of the most widely used kernel functions for nonlinear problems, which is expressed as follows (Burges, 1998):

$$k\left(\mathbf{x}_i, \mathbf{x}_j\right) = \exp\left(-\gamma \left\|\mathbf{x}_i - \mathbf{x}_j\right\|^2\right) \tag{22}$$

Here, $\gamma$ is a kernel parameter defined by the user.

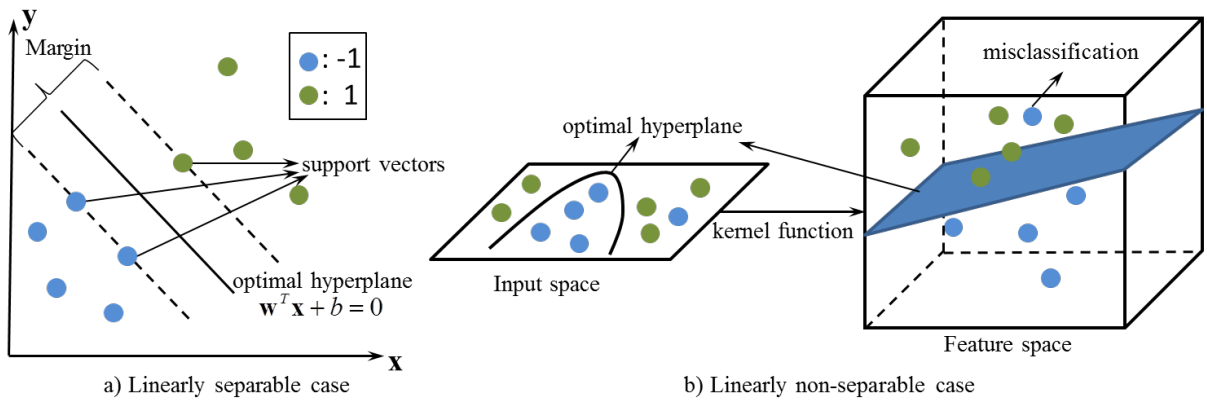


Figure 10 Linear and nonlinear SVM models

The procedure of applying an SVM to the case study is shown in Figure 11. The first and last steps are similar to those for the application of an ANN. Steps 2-4 are introduced to search for the optimum combination of the kernel's parameter $\gamma$ and soft margin parameter $C$, which are two important parameters determining the performance of the SVM model. Many computer codes for SVM training are readily available online, e.g., the LIBSVM compiled by Chang and Lin (2011), LS-SVMlab by Suykens and Vandewalle (1999) and the MATLAB toolbox fitcsvm, which is used in this study.

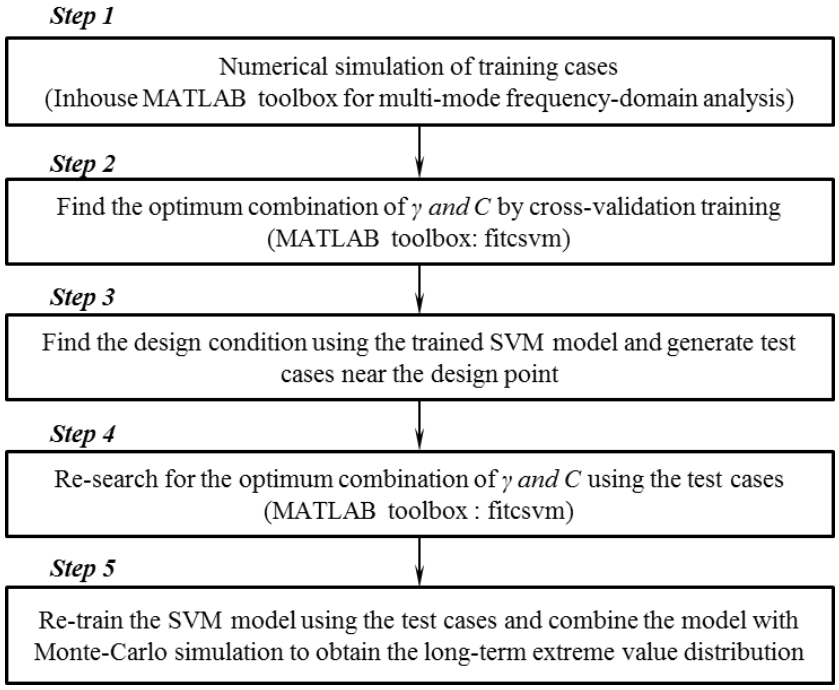


Figure 11 The procedure of the application of an SVM for predicting long-term extreme load effects

### 3.6.3.1 Determination of parameters

Cross-validation technique is used to search for the optimum combination of the hyperparameters $\gamma$ and $C$. The method requires dividing the training data into subsets and calculating an average error quantity. Repeating this with different hyperparameters, the combination of parameters that give the least average error is chosen as the optimal. To that end, the 125 environmental conditions are divided here into eight subsets. Each environmental condition is then grouped with 1001 values of $u_4$. The mean error rate of classifying the 'unknown' set under different combinations of $\gamma$ and $C$ is shown in Figure 12. The SVM model with parameters $\gamma=2^4$ and $C=2^9$ introduces the least error and is used to find the MPP ($u_1$=4.23, $u_2$=0.508, $u_3$=-0.304, and $u_4$=1.84). The test conditions are shown by the yellow circles in Figure 4,

and $u_4$ is selected in the range [-5, 5] with an interval of 0.01. The error rates of the classification of the test cases under different combinations of kernel parameter $\gamma$ and soft margin parameter $C$ are shown in Figure 13. Finally, $\gamma=2^2$ *and* $C=2^{13}$ are selected as the parameters for the model as the combination gives the least error in classification of the test data.

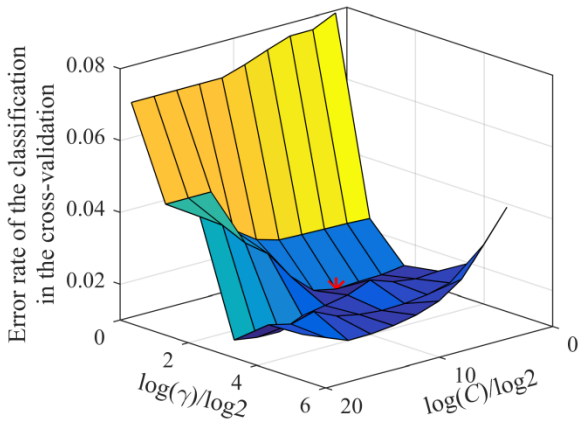


Figure 12 Error rate of the classification of the validation set based on cross-validation

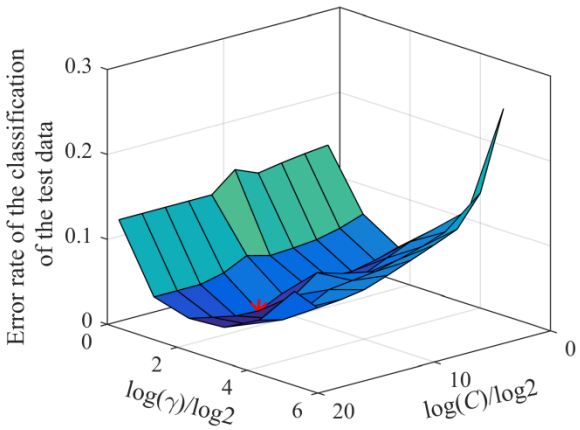


Figure 13 Error rate of the classification of the test cases

### 3.6.3.2 SVM-based Monte Carlo simulation

After determining the parameters, the SVM model is re-trained by adding the test cases to the training cases. The predicted and true failure surfaces are shown in Figure 14. Similar to the case of the ANN-based MC method, there is a good agreement between the two surfaces. The value of the CDF of the extreme bending moment according to the Monte Carlo simulation is 0.402 with an error of 1.41% compared to the results obtained using the full long-term method.

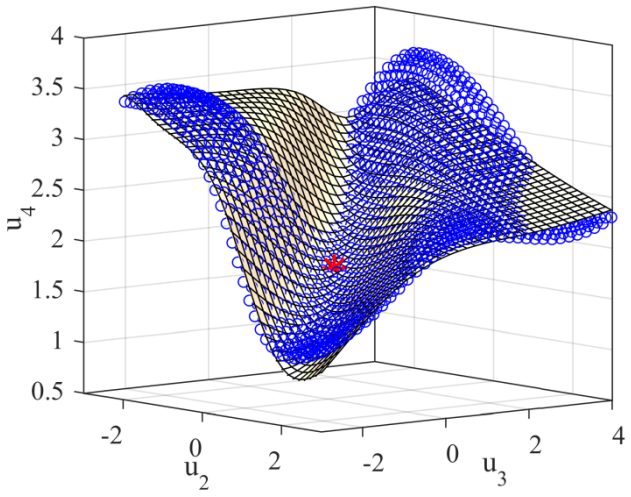


Figure 14 Comparison of the failure surface between the SVM and exact solutions. (o Failure surface based on SVM; — exact failure surface; * design case)

### 3.6.4 The effect of the randomness and size of the training data

The random nature of the training data can affect the training process and consequently the performance of the ANN and SVM models. For instance, if the randomly generated environmental conditions for

training are near the design point by chance, the predicted results will likely match well with the true values. To guarantee that the better performance of the machine learning approaches over traditional reliability analysis methods is not owed to coincidence, three different training cases with different sizes are generated. Table 3 and Table 4 show the cumulative probabilities of the long-term extreme values corresponding to the bending moment value of 50.42 MNm and the corresponding errors along with a comparison of the failure surface.

For the ANN-based method, 3×3×3 environmental conditions are not sufficient to predict the probability distribution of the long-term extreme values. The variation in the CDF value based on the three different random training sets is large, and the agreement between the failure surfaces is poor. When the number of training environmental conditions is increased to 4×4×4, the ANN gives satisfactory predictions. The maximum error is found to be 7.12%; therefore, the accuracy is not a result of a 'cancellation effect' because the failure surfaces also match well. Thus, only 73 environmental conditions are required including the test conditions, which is fewer than that in FORM. The performance becomes significantly better when 5×5×5 and 6×6×6 training conditions are used.

The performance of the trained SVM model is presented in Table 4. The prediction becomes satisfactory as the number of training environmental conditions increases to 5×5×5, where 3×3×3 conditions are clearly not enough. Although the CDF of long-term extreme response is accurate based on the first two random sets of 4×4×4 conditions, it should be attributed to the cancellation effect according to the poor match of the failure surface.

### 3.7 Comparison of the failure probability based on different approaches

The probability of the extreme values of the bending moment below 50.42 MNm in 100 years and the number of simulations required for the full long-term method, FORM, SORM, ANN-Monte Carlo, and SVM-Monte Carlo approaches are compared in Table 5. FORM requires the simulation of 78 environmental conditions; 65 of these conditions come from 13 iterations, whereas the other 13 are performed due to backtracking to guarantee the convergence. SORM requires ten more to calculate the elements in the Hessian matrix.

In this case study, the performance of the ANN in predicting the probability of the long-term extreme load effects of suspension bridges with floating pylons is better than those of the FORM and SORM from the perspective of both computational efficiency and accuracy. Another advantage of applying the machine learning approach is that the numerically simulated cases can also be used to predict the CDF at any specified extreme value for different response parameters.

The SVM is not as good as the ANN method because regression is performed in the ANN, whereas a classification algorithm is employed in the SVM. Therefore, the targets of the training cases in the ANN are the long-term extreme values, whereas in the SVM, the target values are simply '-1' and '1', representing failure and safety, respectively. Therefore, much more information is efficiently used in the neural networks.

Table 3 Effect of the size and uncertainty of the training data in the ANN

| 3x3x3 training conditions + 9 test conditions | | | 4x4x4 training conditions + 9 test conditions | | |
|---|---|---|---|---|---|
| CDF value of the long-term extreme value and error | | | CDF value of the long-term extreme value and error | | |
| Training set 1 | Training set 2 | Training set 3 | Training set 1 | Training set 2 | Training set 3 |

| | | | | | |
|---|---|---|---|---|---|
| 0.4162 | 0.3021 | 0.4449 | 0.3678 | 0.3843 | 0.3881 |
| 5.10% | 23.7% | 12.3% | 7.12% | 2.95% | 1.99% |

comparison of the failure surface using training set 1

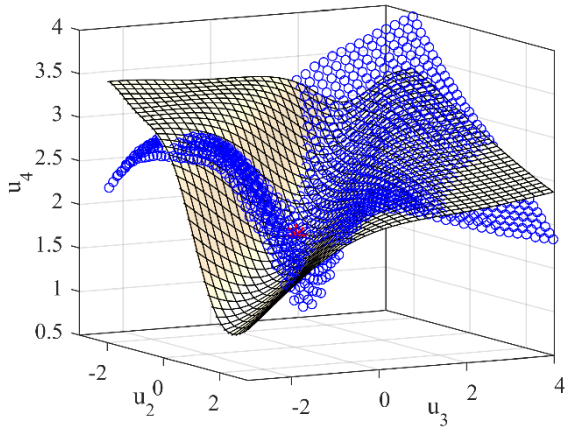


5x5x5 training conditions + 9 test conditions

CDF value of the long-term extreme value and error

| Training set 1 | Training set 2 | Training set 3 |
|---|---|---|
| 0.3985 | 0.3963 | 0.3999 |
| 0.631% | 0.076% | 0.985% |

comparison of the failure surface using training set 2

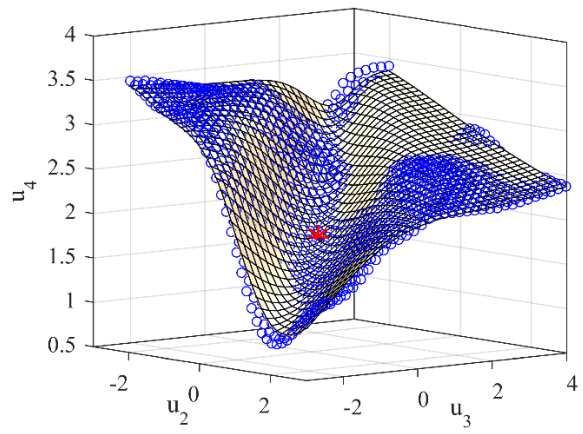


comparison of the failure surface using training set 3

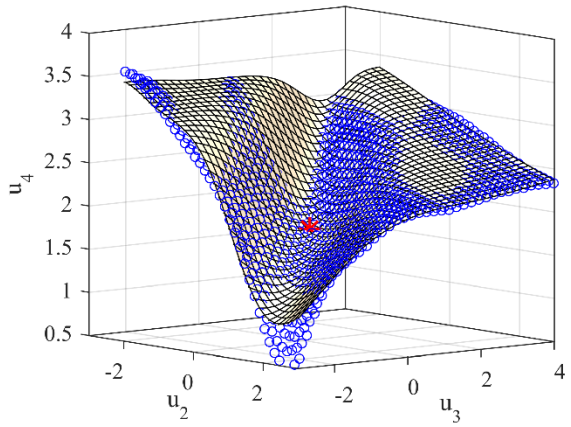


6x6x6 training conditions + 9 test conditions

CDF value of the long-term extreme value and error

| Training set 1 | Training set 2 | Training set 3 |
|---|---|---|
| 0.3958 | 0.3893 | 0.3909 |
| 0.051% | 1.69% | 1.29% |

comparison of the failure surface using training set 1

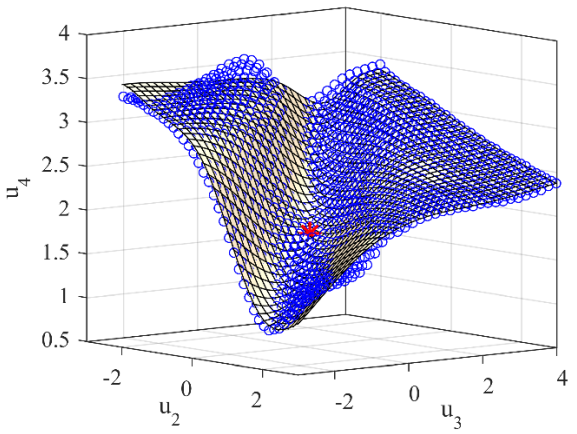


Table 4 Effect of the size and uncertainty of the training data in the SVM

| 3x3x3 training conditions + 9 test conditions | | | 4x4x4 training conditions + 9 test conditions | | |
|---|---|---|---|---|---|
| CDF value of the long-term extreme value and error | | | CDF value of the long-term extreme value and error | | |
| Training set 1 | Training set 2 | Training set 3 | Training set 1 | Training set 2 | Training set 3 |

| | | | | | |
|---|---|---|---|---|---|
| 0.3323 | 0.3457 | 0.4373 | 0.3605 | 0.3742 | 0.2909 |
| 16.0% | 12.7% | 10.4% | 8.96% | 5.50% | 26.5% |
| comparison of the failure surface using training set 3 | | | comparison of the failure surface using training set 2 | | |

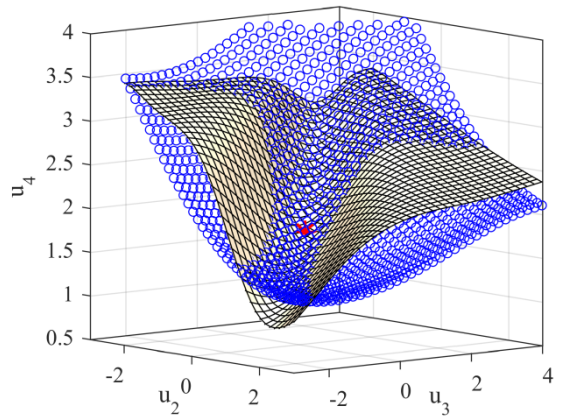


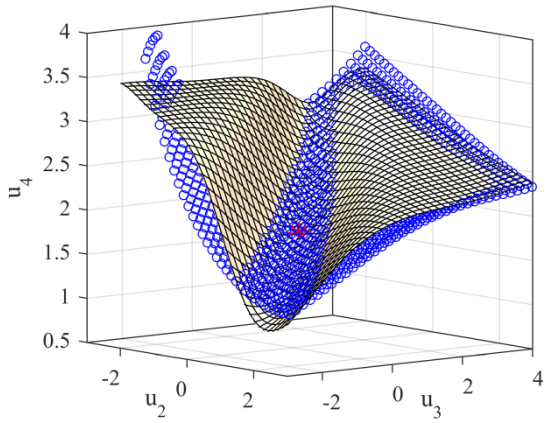


| 5x5x5 training conditions + 9 test conditions | | | 6x6x6 training conditions + 9 test conditions | | |
|---|---|---|---|---|---|
| CDF value of the long-term extreme value and error | | | CDF value of the long-term extreme value and error | | |
| Training set 1 | Training set 2 | Training set 3 | Training set 1 | Training set 2 | Training set 3 |
| 0.3793 | 0.3953 | 0.3436 | 0.3847 | 0.4116 | 0.3710 |
| 4.22% | 0.177% | 13.2% | 2.85% | 1.69% | 6.31% |
| comparison of the failure surface using training set 2 | | | comparison of the failure surface using training set 2 | | |

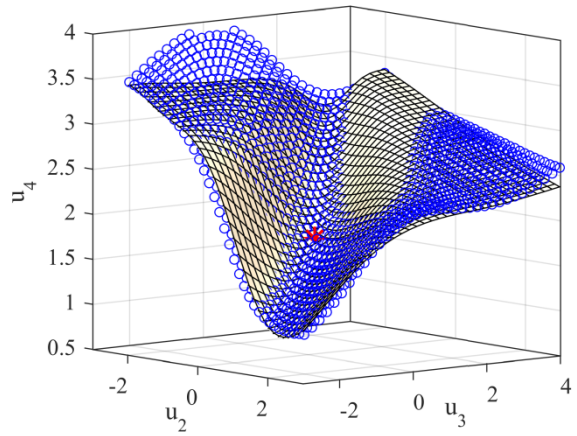


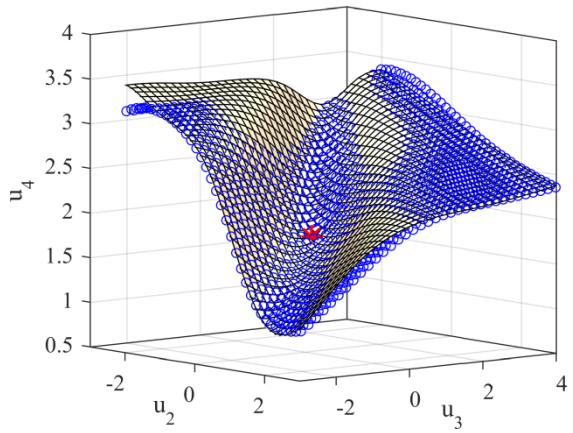


Table 5 Comparison of the cumulative probabilities and computational effort for different methods

| Method | CDF value | Cases required | Error (%) |
|---|---|---|---|
| Full long-term | 0.396 | / | / |
| FORM | 0.228 | 5*13+13=78 | 39.5 |
| SORM | 0.441 | 78+10=88 | 10.3 |
| ANN-based Monte Carlo simulation | 0.416 / 0.302 / 0.445 | 3×3×3+9=36 | 5.1 / 23.7 / 12.3 |
| | 0.368 / 0.384 / 0.388 | 4×4×4+9=73 | 7.12 / 2.95 / 1.99 |
| | 0.399 / 0.396 / 0.400 | 5×5×5+9=134 | 0.63 / 0.076 / 0.99 |

| | | | |
|---|---|---|---|
| | 0.396 / 0.390 / 0.391 | 6×6×6+9=225 | 0.051 / 1.69 / 1.29 |
| SVM-based Monte Carlo simulation | 0.332 / 0.346 / 0.437 | 3×3×3+9=36 | 16.0 / 12.7 / 10.4 |
| | 0.361 / 0.374 / 0.291 | 4×4×4+9=73 | 8.96 / 5.5 / 26.5 |
| | 0.379 / 0.395 / 0.344 | 5×5×5+9=134 | 4.22 / 0.177 / 13.2 |
| | 0.385 / 0.412 / 0.371 | 6×6×6+9=225 | 2.85 / 1.69 / 6.31 |

## 4 Conclusions

The machine learning methods of the ANN-based and SVM-based Monte Carlo simulations are applied to a case study of long-term extreme load effects on a suspension bridge with floating pylons under combined wind and wave actions. A comparison between machine learning methods and first- and second-order reliability methods is conducted to determine the computational accuracy and efficiency of the methods in calculation of the cumulative probabilities of the long-term extreme values of the bending moment due to vertical deflections at the critical position of the girder.

In the case study of the suspension bridge with floating pylons, which is characterized by a strongly nonlinear limit state function, first- and second-order Taylor expansions are not found sufficiently accurate. The ANN regression algorithm yields more accurate results than the SORM when similar number of environmental conditions are used. The SVM classification algorithm requires more computational effort than the ANN to perform with similar accuracy. Therefore, the ANN approach is recommended based on the case study results.

Another reason for recommending the ANN method is that the long-term cumulative probability of any specified short-term extreme peak value can be achieved through only one training process. It can be further used to calculate the characteristic long-term extreme response values for ULS and ALS design checks. To achieve the same goal, FORM, SORM, and SVM training have to be repeated several times at different specified critical response values. Consequently, the computational effort required will be significantly larger compared to the ANN-based method.

## 5 Acknowledgments

This research was conducted with financial support from the Norwegian Public Roads Administration. The authors gratefully acknowledge this support.

## 6 References

Breitung, K., 1984. Asymptotic approximations for multinormal integrals. J. Eng. Mech. https://doi.org/10.1061/(ASCE)0733-9399(1984)110:3(357)

Burges, C.J.C., 1998. A tutorial on support vector machines for pattern recognition. Data Min. Knowl. Discov. https://doi.org/10.1023/A:1009715923555

Cardoso, J.B., de Almeida, J.R., Dias, J.M., Coelho, P.G., 2008. Structural reliability analysis using Monte Carlo simulation and neural networks. Adv. Eng. Softw. https://doi.org/10.1016/j.advengsoft.2007.03.015

Chang, C.C., Lin, C.J., 2011. LIBSVM: A Library for support vector machines. ACM Trans. Intell. Syst. Technol. https://doi.org/10.1145/1961189.1961199

Charalambous, C., 1992. Conjugate gradient algorithm for efficient training of artificial neural networks. IEE Proceedings, Part G Circuits, Devices Syst. https://doi.org/10.1049/ip-g-2.1992.0050

Dan Foresee, F., Hagan, M.T., 1997. Gauss-Newton approximation to bayesian learning, in: IEEE International Conference on Neural Networks - Conference Proceedings. https://doi.org/10.1109/ICNN.1997.614194

Der Kiureghian, A., Dakessian, T., 1998. Multiple design points in first and second-order reliability. Struct. Saf. 20, 37–49. https://doi.org/10.1016/S0167-4730(97)00026-X

Der Kiureghian, A., De Stefano, M., 1991. Efficient algorithm for second-order reliability analysis. J. Eng. Mech. https://doi.org/10.1061/(ASCE)0733-9399(1991)117:12(2904)

Du, X., 2005. First order and second reliability methods. Probabilistic Eng. Des. https://doi.org/10.1137/090771181

Gong, S.W., Halden, S., 2016. Dynamic Response of Suspension Bridge with Floating Towers. NTNU.

Hagan, M.T., Menhaj, M.B., 1994. Training Feedforward Networks with the Marquardt Algorithm. IEEE Trans. Neural Networks. https://doi.org/10.1109/72.329697

Hasofer, A.M., Lind, N.C., 1974. EXACT AND INVARIANT SECOND-MOMENT CODE FORMAT. ASCE J Eng Mech Div.

Haver, S., Winterstein, S.R., 2009. Environmental contour lines: A method for estimating long term extremes by a short term analysis. Trans. - Soc. Nav. Archit. Mar. Eng.

Hirschen, K., Schäfer, M., 2006. Bayesian regularization neural networks for optimizing fluid flow processes. Comput. Methods Appl. Mech. Eng. https://doi.org/10.1016/j.cma.2005.01.015

Hurtado, J.E., 2004. An examination of methods for approximating implicit limit state functions from the viewpoint of statistical learning theory. Struct. Saf. https://doi.org/10.1016/j.strusafe.2003.05.002

Johannessen, K., Meling, T.S., Haver, S., 2002. Joint distribution for wind and waves in the Northern North Sea. Int. J. Offshore Polar Eng.

Li, H.S., Lu, Z.Z., Yue, Z.F., 2006. Support vector machine for structural reliability analysis. Appl. Math. Mech. (English Ed. https://doi.org/10.1007/s10483-006-1001-z

Li, L., Gao, Z., Moan, T., 2015. Joint Distribution of Environmental Condition at Five European Offshore Sites for Design of Combined Wind and Wave Energy Devices. J. Offshore Mech. Arct. Eng. https://doi.org/10.1115/1.4029842

Liang, F., 2005. Bayesian neural networks for nonlinear time series forecasting. Stat. Comput. https://doi.org/10.1007/s11222-005-4786-8

Liu, P.L., Der Kiureghian, A., 1991. Optimization algorithms for structural reliability. Struct. Saf. https://doi.org/10.1016/0167-4730(91)90041-7

MacKay, D.J.C., 1992a. Bayesian Interpolation. Neural Comput. https://doi.org/10.1162/neco.1992.4.3.415

MacKay, D.J.C., 1992b. A Practical Bayesian Framework for Backpropagation Networks. Neural Comput. https://doi.org/10.1162/neco.1992.4.3.448

Madsen, H.O., Krenk, S., Lind, N.C., 2006. Methods of Structural Safety, Dover Civil and Mechanical Engineering Series. Dover Publications.

Naess, A., Moan, T., 2012. Stochastic Dynamics of Marine Structures. Cambridge University Press, Cambridge. https://doi.org/DOI: 10.1017/CBO9781139021364

Pan, Q., Dias, D., 2017. An efficient reliability method combining adaptive Support Vector Machine and Monte Carlo Simulation. Struct. Saf. https://doi.org/10.1016/j.strusafe.2017.04.006

Papadrakakis, M., Papadopoulos, V., Lagaros, N.D., 1996. Structural reliability analyis of elastic-plastic structures using neural networks and Monte Carlo simulation. Comput. Methods Appl. Mech. Eng. https://doi.org/10.1016/0045-7825(96)01011-0

Rackwitz, R., Flessler, B., 1978. Structural reliability under combined random load sequences. Comput. Struct. https://doi.org/10.1016/0045-7949(78)90046-9

Rocco, C.M., Moreno, J.A., 2002. Fast Monte Carlo reliability evaluation using support vector machine. Reliab. Eng. Syst. Saf. https://doi.org/10.1016/S0951-8320(02)00015-7

Rosenblatt, M., 1952. Remarks on a Multivariate Transformation. Ann. Math. Stat. https://doi.org/10.1214/aoms/1177729394

Rumelhart, D.E., Hinton, G.E., Williams, R.J., 1986. Learning representations by back-propagating errors. Nature. https://doi.org/10.1038/323533a0

Santos, S.R., Matioli, L.C., Beck, A.T., 2012. New optimization algorithms for structural reliability analysis. C. - Comput. Model. Eng. Sci. https://doi.org/10.3970/cmes.2012.083.023

Suykens, J.A.K., Vandewalle, J., 1999. Least squares support vector machine classifiers. Neural Process. Lett. https://doi.org/10.1023/A:1018628609742

Titterington, D.M., 2004. Bayesian methods for neural networks and related models. Stat. Sci. https://doi.org/10.1214/088342304000000099

Vogl, T.P., Mangis, J.K., Rigler, A.K., Zink, W.T., Alkon, D.L., 1988. Accelerating the convergence of the back-propagation method. Biol. Cybern. https://doi.org/10.1007/BF00332914

Xu, Y., Øiseth, O., Moan, T., 2018a. Time domain simulations of wind- and wave-induced load effects on a three-span suspension bridge with two floating pylons. Mar. Struct. https://doi.org/10.1016/j.marstruc.2017.11.012

Xu, Y., Øiseth, O., Moan, T., Naess, A., 2018b. Prediction of long-term extreme load effects due to wave and wind actions for cable-supported bridges with floating pylons. Eng. Struct. https://doi.org/10.1016/j.engstruct.2018.06.023

Zhang, Y., Kiureghian, A., 1995. Two Improved Algorithms for Reliability Analysis, in: Reliability and Optimization of Structural Systems. https://doi.org/10.1007/978-0-387-34866-7_32

Zhao, H. bo, 2008. Slope reliability analysis using a support vector machine. Comput. Geotech. https://doi.org/10.1016/j.compgeo.2007.08.002

Zhao, Y.G., Ono, T., 1999. A general procedure for first/second-order reliability method (FORM/SORM). Struct. Saf. https://doi.org/10.1016/S0167-4730(99)00008-9